

Robust Low-Level Motion Control of WMR with Stochastic Active Observers

Rodrigo Maia[†], Rui Cortesão[†], Urbano Nunes[†], Valter Silva[‡], José Fonseca[‡]

[†] Institute for Systems and Robotics
University of Coimbra
3030-290 Coimbra - Portugal
{rmaia,cortesao,urbano}@isr.uc.pt

[‡] Dep. Electronics and Telecommunications
University of Aveiro
3810-193 Aveiro - Portugal
vfs@estg.iplei.pt, jaf@det.ua.pt

Abstract

This paper describes a robust control method for the low-level motion of a Wheeled Mobile Robot (WMR). It is demonstrated through simulation analysis that the Active Observer (AOB) Control structure provides a reliable tracking control action, for the WMRs wheel velocity, in spite of parameters uncertainties. The results show that this type of controller structure can be applied to WMR, where information of motor intrinsic parameters or cross-couplings is unavailable, this is the case of robotic wheelchair "RobChair" [1].

1 Introduction

The control of motion systems often involves uncertainty. The AOB [2] is a new control design that imposes a desired closed loop behavior regardless of unmodeled unknown terms. The AOB control structure has been successfully applied in several control applications [3, 4, 5, 6].

A Global Navigation System for WMR is under development at ISR [7]. In this system a four functional levels based model is addressed. The highest level, the *global motion planning*, is responsible for feeding the *local motion planning*, the level directly beneath, with a path to a predefined goal. This local motion planning level is responsible to plan and provide a collision free trajectory in the reference path. This path is received by the *tracking motion level* that determines the velocity commands, minimizing the trajectory tracking error, and sends them to the lowest level, the *motion control level*.

The motion control level is the scope of this work. The paper is organized as follows: section 2 describes a simulation model of this low-level motion; section 3 describes two control strategies for this motion control level, one that uses a model of the system considering actuator dynamics and cross-coupling information, to produce the command signals of both actuators. The second uses two decoupled models, one for each wheel, together with an AOB control structure to drive the

robot with a desired behavior. Section 4 presents the results achieved with both controllers. Their performance is analyzed. In section 5, a Distributed Embedded System (DES) that supports the control loop, is presented.

2 The Simulation Model

To produce a thorough analysis of the behavior of the low-level motion of a WMR, a realistic simulation model has to be designed. The low-level motion system of a WMR comprises two Digital-to-Analog Converters (DAC), two power drives, two permanent magnet DC motors, two gear boxes, two optical encoders, and the robot frame.

WMR's motion is obtained through actuation of the motors attached to each drive wheel. The block diagram in Figure 1 proposes a decomposition for the typical Permanent Magnet DC Motor based in the one described by Nørgard et al. [8].

The diagram considers the motor friction as a sum of one linear term, the viscous friction, and two nonlinear terms, the coulomb friction and the stiction. The the load torque related to the viscous friction (τ_{vf}) is given by:

$$\tau_{vf} = B\omega_m, \quad (1)$$

where B is a constant and ω_m is the motor angular velocity. The coulomb friction τ_{cf} and the stiction τ_s related torques are nonlinear equations,

$$\tau_{cf} = T_{cf} \cdot \text{sign}(\omega_m) \quad (2)$$

and

$$\tau_s = \begin{cases} \text{sign}(\omega_m) \cdot \min(T_s, |\tau_m - \tau_l|) & \text{if } \omega_m = 0 \\ 0 & \text{if } \omega_m \neq 0 \end{cases}, \quad (3)$$

(T_{cf} is the coulomb friction absolute value and T_s denotes the maximum stiction) which are inapplicable in a simulation model, however in [8] it is also proposed a friction model that provides a reasonable trade-off between accuracy and simulation speed.

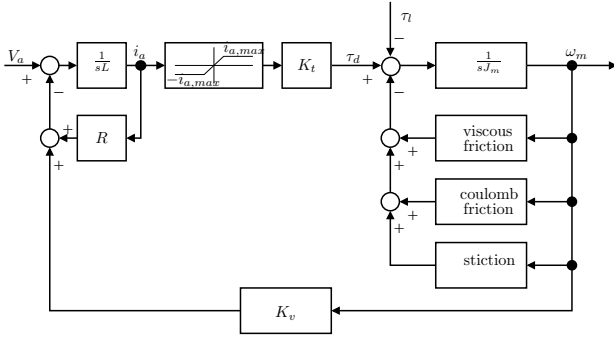


Figure 1: Permanent Magnet DC Motor Block Diagram

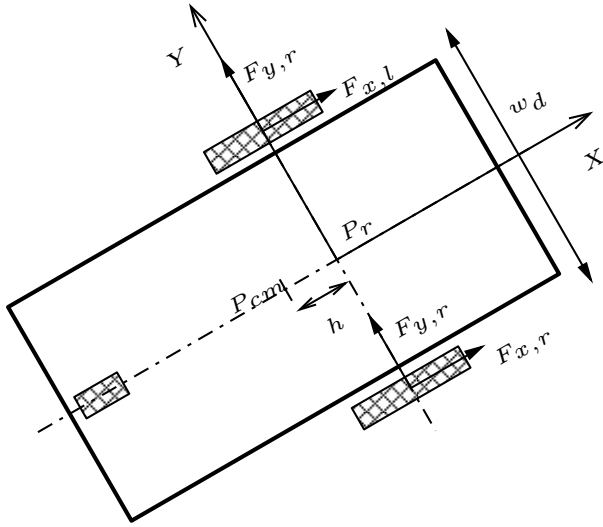


Figure 2: Generic Differential Drive Wheeled Mobile Robot Model

Considering DAC's (K_{DAC}), power drive's (K_{Drive}) and encoder's (K_{enc}) gains, Figure 1 and equations (1)-(3), the input-output relation of each wheel actuator is given by

$$\begin{aligned} \frac{J_m}{K_{enc}} \dot{\omega}_{enc} &= \frac{K_{DAC} K_{Drive} K_\tau}{R} u - \\ &- \frac{B}{K_{enc}} \omega_{enc} - \frac{K_v K_\tau}{K_{enc} R} \omega_{enc} - \\ &- T_{cf} \cdot \text{sign}(\omega_{enc}) - T_s - \tau_l, \end{aligned} \quad (4)$$

where J_m is the motor shaft inertia, K_v and K_τ are the motor voltage and torque constants, and u is the signal issued to the DAC.

When analyzing the motion of Differential Drive WMR it is recognized that the motion of one of the actuated wheels will induce a motion in the other. This effect is due to the *dynamic coupling* resultant of the coupled motions, of both wheels, through the robot rigid body [9].

The motion of rigid system are commonly described as a sum of translations and rotations. The translational motion is ruled by the Linear Momentum The-

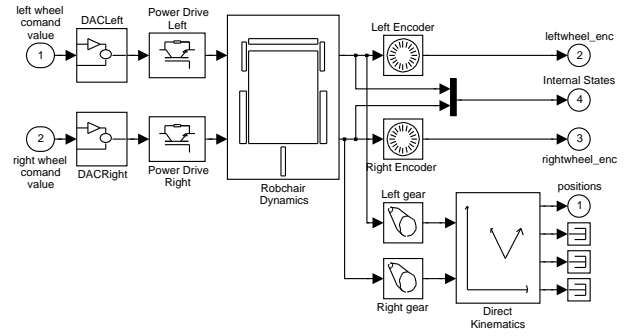


Figure 3: Simulink® Block Diagram of a WMR Motion Model

orem, and the rotational by the Angular Momentum Theorem. Based on this, Andersen [9] and Nørgard et al. [8] have proposed a model, as the one in Figure 2, to the torque associated with each wheel of a Differential Drive WMR. In this model, the load torque for each wheel are

$$\begin{aligned} \tau_{l,l} &= K_{ll} \dot{\omega}_{m,l} + K_{lr} \dot{\omega}_{m,r} + \\ &+ K_{lrr} \omega_{m,r}^2 - K_{llr} \omega_{m,r} \omega_{m,l} \end{aligned} \quad (5)$$

$$\begin{aligned} \tau_{l,r} &= K_{lr} \dot{\omega}_{m,l} + K_{rr} \dot{\omega}_{m,r} + \\ &+ K_{llr} \omega_{m,l}^2 - K_{lrr} \omega_{m,r} \omega_{m,l} \end{aligned} \quad (6)$$

where

$$\begin{aligned} K_{ll} &= \frac{r_l^2}{N^2} \left(\frac{M}{4} + \frac{J+Mh^2}{w_d^2} \right), & K_{llr} &= \frac{Mhr_l r_r^2}{w_d^2 N^3}, \\ K_{rr} &= \frac{r_r^2}{N^2} \left(\frac{M}{4} + \frac{J+Mh^2}{w_d^2} \right), & K_{lrr} &= \frac{Mhr_l^2 r_r}{w_d^2 N^3}, \\ K_{lr} &= \frac{r_r r_l}{N^2} \left(\frac{M}{4} - \frac{J+Mh^2}{w_d^2} \right). \end{aligned} \quad (7)$$

The first two terms (in (5) and (6)) are components of the *angle acceleration force*, and the last two are components of the *Coriolis* and *Centrifugal forces* respectively.

To perform the simulation of the complete model (4) the *Simulink*® block diagram, presented in Figure 3 was developed.

3 Controller Design

This section presents two control strategies to control the wheel velocity of a WMR.

3.1 Coupled Model

Considering the Multiple-Input-Multiple-Output model of the system obtained by substitution of (5)-(6) in (4), and neglecting the non-linear terms (τ_s , τ_{cf} , and Coriolis and centrifugal forces), the following two-input-two-output state-space model is achieved:

$$\begin{bmatrix} \dot{\omega}_{m,l}(t) \\ \dot{\omega}_{m,r}(t) \end{bmatrix} = A \begin{bmatrix} \omega_{m,l}(t) \\ \omega_{m,r}(t) \end{bmatrix} + B \begin{bmatrix} u_l(t) \\ u_r(t) \end{bmatrix} \quad (8)$$

the real step response, that was used to calculate the model parameters. However these values of P_{TF} and K_{TF} can be used as a starting point in a recursive process that minimizes the mean square error between real and simulated step responses.

It is desired to have a steady-state error for a step input. To accomplish this goal the Loop Transfer Function (LTF) must have at least one pole at the origin, which is not the present case (type 0 system). Therefore, an artificial integrator at the plant input was inserted (see Figure 5).

The extended plant has the TF given by,

$$H(s) = \frac{\Omega_{enc}(s)}{U(s)} = \frac{K_{LTF}}{s(s + P_{LTF})}, \quad (16)$$

that leads to the state-space model:

$$\dot{x}(t) = \begin{bmatrix} 0 & 1 \\ -P_{LTF} & 0 \end{bmatrix} x(t) + \begin{bmatrix} 0 \\ K_{LTF} \end{bmatrix} u(t) \quad (17)$$

and

$$y(t) = [1 \ 0] x(t), \quad (18)$$

where $y(t) = \omega_{enc}(t)$. Discretizing (17)-(18) with a sample time h , results

$$\begin{aligned} x_{\kappa+1} &= \Phi x_{\kappa} + \Gamma u_{\kappa} \\ y_{\kappa} &= C x_{\kappa} \end{aligned}, \text{ with } \begin{aligned} \Phi &= e^{Ah} \\ \Gamma &= \int_0^h e^{As} B \end{aligned}, \quad (19)$$

where A , B and C are the state transition, command and measurement matrices of (17)-(18), respectively.

A critically damped behavior is desired for this system, which can be designed through proper state feedback [10, 11].

The L_c gain it is necessary to ensure an unitary DC gain (see Figure 5). Considering the Final Value Theorem, L_c is computed by

$$L_c = \frac{1}{C(I - (\Phi - \Gamma L))^{-1} \Gamma}. \quad (20)$$

The estimation of the system state, necessary to the state feedback controller, is done by the AOB. The AOB issues also an extra state, the active state p_{κ} , that must compensate all modeling errors referred to the system input. The AOB structure and algorithm is described in detail in [2, 3, 4].

The state estimation is:

$$\begin{aligned} \hat{x}_{\kappa} &= \Phi_c \hat{x}_{\kappa-1} + \Gamma_a r_{\kappa-1} + \\ &+ K_{\kappa} [y_{\kappa} - C(\Phi_c \hat{x}_{\kappa-1} + \Gamma_a r_{\kappa-1})], \end{aligned} \quad (21)$$

where

$$\begin{aligned} \Phi_c &= \Phi_a - \Gamma_a [L \ 1], \\ \Gamma_a &= \begin{bmatrix} \Gamma \\ 0 \end{bmatrix} \text{ and } \Phi_a = \begin{bmatrix} \Phi & \Gamma \\ 0 & 1 \end{bmatrix}. \end{aligned} \quad (22)$$

M	55 kg	J	5.46 kg·m ²
w_d	0.54 m	R	0.588 Ω
h	0.12 m	L	0.001 H
K_{enc}	127.324	B	$4.6 \times 10^{-5} \frac{\text{Nm}}{\text{rad}}$
N	36	$T_{cf} = T_s$	0.066 N·m
K_{DAC}	0.0049	J_m	0.000263 kg·m ²
K_{Drive}	2	$K_v = K_{\tau}$	0.0293 $\frac{\text{Vs}}{\text{rad}}$
$i_{a_{max}}$	5.5 A		

Table 1: Simulation Parameters

L is obtained by the Ackerman's Formula to achieve a desired closed loop behavior.

The observer gain K_{κ} is computed through the Kalman filter algorithm using the system matrices Φ_a and Γ_a . The used measurement (R) and system (Q) noise matrices are

$$R = \begin{bmatrix} \frac{1}{12K_{enc}^2} \end{bmatrix} \text{ and } Q = \begin{bmatrix} 10^{-12} & 0 & 0 \\ 0 & 10^{-12} & 0 \\ 0 & 0 & 10^{-4} \end{bmatrix}. \quad (23)$$

The diagonal components of the Q matrix represent the uncertainty of the model for each state. For the states x_1 (velocity) and x_2 (acceleration) uncertainty is low (model reference control), for the p_{κ} state the uncertainty is high to cope with unmodeled terms.

4 Performance Analysis

Figures 6 and 7 present simulation results for the model of Figure 3. The parameters used are, shown in Table 1. Equal motors were considered. The results in Figure 6 are the velocities of the wheels (v_{left} and v_{right}) when a reference vector r (r_{left} and r_{right}) is applied. At $t = 5$ s a parametric disturbance is introduced in the system. The WMR mass and inertia are reduced to half of their values. Figure 6.a shows that with the two DOF controller the response of both wheels, prior to the parametric disturbance, is as expected (critically damped). After the parametric disturbances an overshoot appears when a new step is applied. With the AOB (Figure 6.b) this effect is unnoticeable. This is due to the adaptive model reference control structure of the AOB. The parametric disturbance is properly compensated by the active state p_{κ} , reducing in this way its influence in the system response.

Figure 7 presents the results of both controllers with a square wave external disturbance (additive to the plant input), with an amplitude of 0.24 V with 5 Hz frequency. The benefit of AOB control structure (Figure 7.b) is notorious, the two DOF controller (Figure 7.a) cannot track correctly the reference.

Another important aspect is that, the cross-couplings between both wheels were not considered

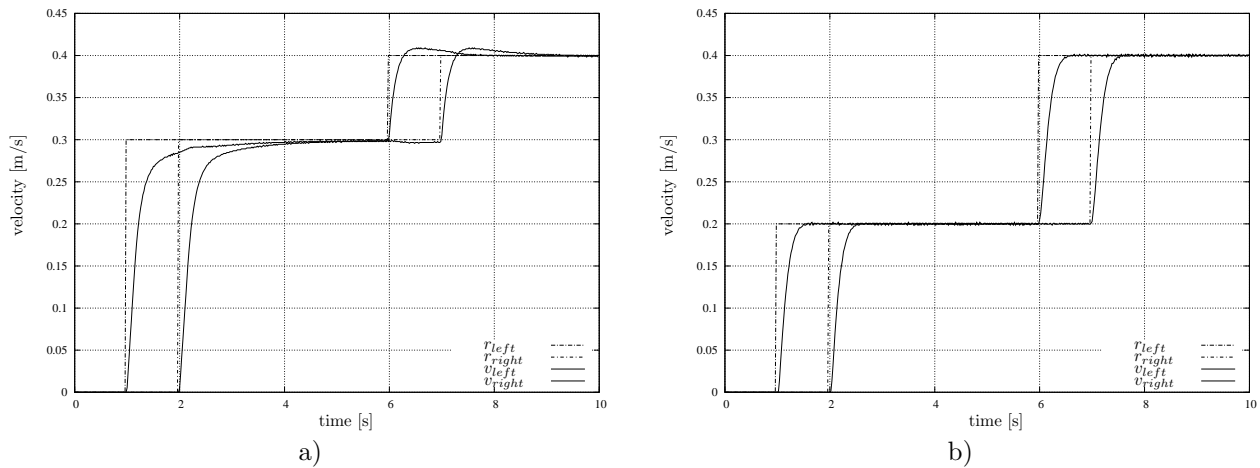


Figure 6: Simulation Results. Velocity response with parametric disturbances. a) Results with the two DOF control; b) Results with the AOB control structure

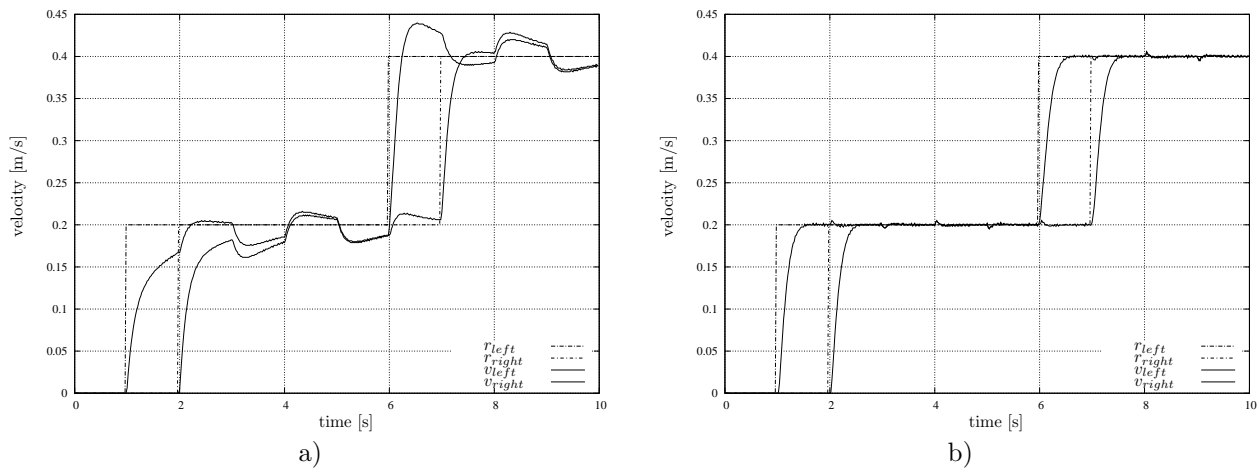


Figure 7: Simulation Results. Velocity response with an input disturbance (square wave). a) Results with the two DOF control; b) Results with the AOB control structure

in the AOB design (decoupled control). However, the overall control performance is not affected.

5 Distributed Architecture

The WMR construction will become much simpler if a Distributed Embedded System (DES) replaces the usual centralized control system. The main benefit comes from the strong reduction in cabling and, consequently, in weight. This issue was also the motivation for the introduction of such systems in automotive industries [12]. The use of a DES has also the benefit of improving system's modularity. It is possible then to start with an architecture that covers just the basic control requirements and that may evolve in the future to add other functionalities. Of course, one has to pay attention to timeliness and dependability issues due to the safety criticality of the envisaged applications. However, for some DESs such

as the ones based in CAN - Controller Area Network (at this moment the de facto standard for automotive industries, even if a new protocol, called FlexRay [13], is ready to replace it) this subject has already been treated. In what concerns timeliness, one can refer, as examples, the work of [14], concerning the worst case response time of messages and the work of [15], concerning the use of protocols to accommodate periodic and sporadic messages without jeopardizing timeliness. A discussion of safety critical issues for automotive industries can be found in [16].

The extensive work around CAN led to adopt it for now as the backbone of the DES architecture for the WMR. In order to define the processing power for the different type of nodes, it is required to map the different functionalities. These are: to acquire the encoders outputs (one for each motor); to impose the power modules setpoints; to input the IR and ultra-

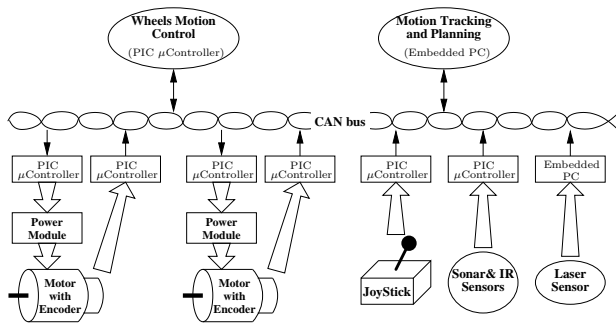


Figure 8: Distributed architecture

sound sensing data; to receive commands from the joystick; to execute the low-level motion control algorithms; to receive and process data from the laser range measurement system; to execute the tracking motion control; to execute motion planning.

The first five functionalities do not require a large processing power and thus small microcontrollers can be used. The new PIC 18F258 from Microchip was adopted. This micro controller can operate up to 40 Mhz and can be configured to use several different I/O systems such as serial ports, ADCs, parallel ports and I2C. This micro-controller has already a CAN interface built-in.

For the other three functionalities, the nodes require more processing power, and then, an industrial embedded PC can be use. The global architecture of the system is shown in Figure 8.

As it can be seen from the Figure 8 , using this kind of system all the nodes share the same communication medium and, as it was said, less wire complexity can be obtained. The mapping of the functionalities in the nodes was done in order to limit each node to only treat a simple signal and make some communication interface. Thus, the need for processing power is kept low or, at least limited. The development of software becomes simpler because one must only concentrate in a simpler functionality in each node. The use of adequate protocols can, after, guarantee composability in what concerns keeping the timeliness of the overall control system [17].

6 Conclusions

A simulation model of the WMR low-level motion has been presented. This model considers nonlinear cross-couplings, nonlinear motor friction terms, and quantization factors due to DACs and encoders.

Two control strategies have been tested to control the WMR wheel velocities. The first is a two DOF controller design that uses a coupled model of the motion. It has a classical Kalman Filter to estimate the

system state, and uses an extended state to provide integral action. The other is based on the AOB control structure and uses two decoupled linear models of the wheel actuators. Simulation results have shown the superior performance of the AOB when parametric or external disturbances actuate in the system.

A Distributed Embedded System has been presented to replace the usual centralized control system of the WMR and suport the control loop presented.

Acknowledgments

This work was partially supported by FCT (Portuguese Science and Technology Foundation) project POSI/33594/SRI/2000, co-financed by the European FEDER Program.

References

- [1] G. Pires and U. Nunes, "A wheelchair steered through voice commands and assisted by a reactive fuzzy-logic controller," *International Journal of Intelligent and Robotic Systems*, vol. 34, pp. 301–314, Junho 2002.
- [2] R. Cortesão, *Kalman Techiniques for Intelligent Control Systems: Theory and Robotic Experiments*. PhD thesis, University of Coimbra, Coimbra, Portugal, 2002.
- [3] R. Cortesão, R. Koeppe, U. Nunes, and G. Hirzinger, "Explicit force control for manipulators with active observers," in *Proceedings of the IEEE Int. Conf. on Intelligent Robots and Systems (IROS'2000)*, vol. 2, (Japan), pp. 1075–1080, 2000.
- [4] R. Cortesão, R. Koeppe, U. Nunes, and G. Hirzinger, "Compliant motion control with stochastic active observers," in *Proceedings of the IEEE Int. Conf. on Intelligent Robots and Systems (IROS'2001)*, (USA), pp. 1876–1881, 2001.
- [5] J. Park, R. Cortesao, and O. Khatib, "Robust and adaptive teleoperation for compliant motion tasks," in *Proceedings of the IEEE Int. Conf. on Advanced Robotics (ICAR'2003)*, (Coimbra, Portugal), 2003.
- [6] M. Naim, R. Cortesão, M. Hanshield, and T. Bueate, "Robust steering algorithms for steer-by-wire vehicles," in *Proceedings of the IEEE Int. Conf. on Advanced Robotics (ICAR'2003)*, (Coimbra, Portugal), 2003.
- [7] U. Nunes, J. A. Fonseca, L. Almeida, R. Araújo, and R. Maia, "Using distributed systems in real-time control of autonomous vehicles," *Robotica - Cambridge University Press*, vol. 22, May 2003.

- [8] M. Nørgaard, N. Poulsen, and O. Ravn, "Models for iau's autonomous guided vehicle," Tech. Rep. IMM-REP-1997-15, Technical University of Denmark, Lyngby - Denmark, 1997.
- [9] G. Andersen, *Modelling and Control of a Mobile Robot: From Dependent Towards Autonomous System*. PhD thesis, Technical University of Denmark, Lyngby, Denmark, 1995.
- [10] G. Frankiln, J. D. Powell, and M. Workman, *Digital Control of Dynamic Systems*. Menlo Park, USA: Addison Wesley Longman, Inc, Third ed., 1998.
- [11] K. Åström and B. Wittenmark, *Computer-Controlled Systems - Theory and Design*. Information and System Sciences Series, New Jersey: Prentice-Hall International, Inc, Third ed., 1997.
- [12] C. Bichet, "Les standard de communication dans l'automobile," in *Proc. of INNOCAP'99, European Symposium on Sensor Networks and Communications*, (Grenoble, France), April 1999.
- [13] R. Belshner, J. Berwanger, C. Ebner, S. Fluhrer, P. Führer, F. Hartwich, B. Hedenetz, R. Hugel, A. Knapp, J. Krammer, P. Lohrmann, B. Müller, M. Peller, and A. Schedl, *FlexRay Requirements Specifications - Version 1.9.7*.
- [14] K. Tindell and A. Burns, "Guaranteeing message latencies on control area network (can)," in *Proc. of the 1st International CAN Conference (ICC'94)*, (Mainz, Germany), 1994.
- [15] L. Almeida, P. Pedreiras, and J. Fonseca, "The ftt-can protocol: Why and how," *IEEE Transactions on Industrial Electronics*, vol. 49, pp. 1189–1201, December 2002.
- [16] J. Ferreira, P. Pedreiras, L. Almeida, and J. Fonseca, "The ftt-can protocol for flexibility in safety-critical systems," *IEEE Micro*, vol. 22, July/August 2002.
- [17] H. Kopetz, *Real-Time Systems: Design Principles for Dist. Embedded Application*. Kluwer, 1997.